Modelling Simul. Mater. Sci. Eng. **17** (2009) 075008 (14pp) doi:10.1088/0965-0393/17/7/075008

Improved modified embedded-atom method potentials for gold and silicon

Seunghwa Ryu[1], **Christopher R Weinberger**[2], **Michael I Baskes**[3] **and Wei Cai**[2]

[1] Department of Physics, Stanford University, Stanford, CA 94305, USA
[2] Department of Mechanical and Aerospace Engineering, Stanford University, Stanford, CA 94305, USA
[3] University of California, San Diego, La Jolla, CA 92093, USA

Received 11 February 2009, in final form 12 June 2009
Published 14 August 2009
Online at stacks.iop.org/MSMSE/17/075008

Abstract
The modified embedded-atom method interatomic potentials for pure gold and pure silicon are improved in their melting point and latent heat predictions, by modifying the multi-body screening function and the equation of state function. The fitting of the new parameters requires rapid calculations of melting point and latent heat, which are enabled by efficient free-energy methods. The results provide the basis for constructing a cross-potential that will be fitted to the binary gold–silicon phase diagram.

(Some figures in this article are in colour only in the electronic version)

1. Introduction

The directed growth of semiconductor nanowires catalyzed by gold nanoparticles via the vapor–liquid–solid (VLS) mechanism has attracted considerable interest worldwide as a promising way to build nanoscale electronic, optical and chemical-sensing devices [1, 2]. Atomistic simulations of nanowire nucleation and growth by the VLS mechanism have been hindered by the lack of a computationally efficient model that reliably describes the interaction between semiconductor (such as silicon) and metal (such as gold) atoms. The tip of the growing nanowire typically contains thousands of atoms, making it prohibitively expensive for first-principles models. Most of the empirical potential models use different functional forms to describe metallic and covalent bonds. Therefore, these models are applicable to either metals or semiconductors, but not both. For example, the embedded-atom method (EAM) [3] model captures the many-body effect in metals by a function that describes the energy required to embed an atom in the background electron density created by its neighbors. In comparison, the Stillinger–Weber (SW) [4] and Tersoff [5] potentials for silicon use terms that include the angle between two bonds to capture the directional nature of covalent bonds.

The modified embedded-atom method (MEAM) model was proposed to describe both metallic and covalent bonds within the same functional form [6]. It extends the EAM to

include directional bonding by accounting for the spatial distribution of background electron density of neighboring atoms. The MEAM potential has been developed for a large number of metals as well as covalent semiconductors. MEAM potentials for many binary alloys have also been developed [7–9]. The MEAM model has many attractive properties for modeling nanowire growth. For example, it successfully describes the change in the coordination of Si atoms from four-fold (covalent bonding) to six-fold (metallic bonding) at melting [10], as well as the surface energy [11, 12] and surface segregation [13, 14] in metals. Therefore, a promising approach to enable atomistic modeling of VLS growth is to develop a MEAM potential that can be fitted to the binary gold–silicon phase diagram. Given that MEAM potentials for pure gold and pure silicon have already been developed, in principle, we only need to develop the cross-potential between gold and silicon atoms.

However, we found that the existing MEAM models of pure gold and pure silicon have several problems that can adversely affect the binary phase diagram and the modeling of VLS growth. In particular, the MEAM potentials underestimate the melting points of both gold and silicon by about 200 K. There are also significant errors in the prediction of the latent heat, which provides the driving force for the liquid–solid phase transition. This is not surprising because the original MEAM potentials were not fitted to the melting point and the latent heat. The purpose of this paper is to improve the melting point and the latent heat predictions of existing MEAM models of gold and silicon by fine-tuning their parameters without changing the overall functional form. In addition, we monitor the predictions of several other transport and mechanical properties that may influence various stages of the nanowire nucleation/growth/termination process, including the diffusion coefficient, thermal expansion coefficient, generalized stacking fault (GSF) energy and volume change on melting. We make an effort to improve the predictions of these properties in the development of the new MEAM potential. However, when a compromise has to be made, we choose to fit the melting point and the latent heat more accurately at the expense of other properties. In a future paper, we will present an MEAM gold–silicon cross-potential based on the improved MEAM potentials developed here.

The paper is organized as follows. In section 2, we present the limitations of existing MEAM potentials for gold and silicon in their predictions of various thermal and mechanical properties. In section 3, we describe our methods to improve the MEAM potentials and present the results. A brief summary is given in section 4.

2. Problem statement

The main goal of this paper is to adjust the MEAM potentials for gold and silicon to accurately reproduce the melting point and the latent heat. During this process, we also monitor the predictions of the diffusion coefficient, thermal expansion coefficient, GSF energy and volume change on melting. Because these properties may also influence various stages of the nanowire nucleation/growth/termination process, we will try to improve them, but will emphasize the melting point and the latent heat when a compromise is necessary. In this section, we benchmark the original MEAM potentials for gold [6] and silicon [6], as well as the more recent second nearest-neighbor (2nn) MEAM potentials for gold [26] and silicon [22]. First, we give a brief summary of the MEAM model.

The MEAM model describes the potential energy of a collection of atoms located at $\boldsymbol{r}_i$, $i = 1, \ldots, N$, by the following equation:

$$V(\{\boldsymbol{r}_i\}) = \sum_{i=1}^{N} F(\overline{\rho}_i) + \sum_{i=1}^{N-1} \sum_{j=i+1}^{N} S_{ij}\, \phi_{ij}(|\boldsymbol{r}_i - \boldsymbol{r}_j|), \tag{1}$$

Table 1. Model predictions and experimental data [15–17] on thermal and mechanical properties of gold. The computation models include original MEAM [6], EAM [23], 2nn-MEAM [26] and two modifications made in this paper (2nn-MEAM* and 2nn-MEAM†) and first-principles calculation with DFT/LDA [18]. The properties include the melting point T_m (in K), latent heat of fusion L (in kJ mol^{-1}), solid and liquid entropy at the melting point, S_S and S_L (in J mol^{-1} K^{-1}), diffusion constant of the liquid D at T_m (in 10^{-9} m^2 s^{-1}), thermal expansion coefficient α of the solid (in 10^{-6} K^{-1}) at 300 K, ideal shear strength τ_c (in GPa) of the solid at zero temperature and volume change on melting $\Delta V_m/V_{solid}$ (in %). Statistical errors are on the order of the last digit of the presented values.

Au	T_m	L	S_S	S_L	D	α	τ_c	$\Delta V_m/V_{solid}$
MEAM [6]	1120	18.2	77.5	93.7	0.6	2.0	10.7	6.6
EAM [23]	984	8.2	85.7	94.0	1.5	13.5	1.68	1.6
2nn-MEAM [26]	1405	18.0	87.4	100.1	2.3	14.6	4.92	7.8
2nn-MEAM*	1173	11.2	87.7	97.2	2.2	20.8	1.81	5.1
2nn-MEAM†	1337	14.2	87.7	98.3	2.3	17.8	2.71	6.5
Exp't	1337.3	12.6	88.4	97.8	—	14.2	—	5.1
DFT/LDA	—	—	—	—	—	—	1.73	

where F is the embedding function, $\overline{\rho}_i$ is the background electron density at $\boldsymbol{r}_i$, S_{ij} is a multi-body screening factor and ϕ_{ij} is the pair potential between atoms i and j. The pair potential function $\phi_{ij}(r)$ is usually not given explicitly. Instead, it is defined as the function that, when combined with the embedding function, reproduces the universal equation of state (EOS) [21] for the potential energy of the reference crystal structure. While the above functional form is similar to that of EAM [3], MEAM has two main extensions. First, the calculation of the background electron density $\overline{\rho}_i$ in MEAM accounts for the spatial arrangements of the neighboring atoms, in addition to their distance to atom i. Second, the range of the pair potential is cut off by a multi-body screening function S_{ij} that depends on the locations of atoms k that are neighbors of both atoms i and j. The details of the MEAM formalism are well described in the literature [6]. The multi-body screening function S_{ij} is summarized in appendix A because we need to adjust it in this work.

2.1. Limitations of the MEAM gold potential

The original MEAM gold potential [6] and 2nn-MEAM gold potential [26] are fitted to two different sets of experimental elastic constants with about 10% of discrepancy. We choose the more recent 2nn-MEAM gold potential as the starting point of our model. Table 1 shows that the 2nn-MEAM gold potential [6] overestimates the melting point T_m by ∼70 K (5%) and overestimates the latent heat L by ∼6 kJ mol^{-1} (43%). These are the main problems that we will address in this paper. The melting point of pure gold is an important feature of the binary gold–silicon phase diagram. At the same time, the latent heat provides the thermodynamic driving force for melting and crystallization when the temperature deviates from the melting point. Because $L = T_m \cdot (S_L - S_S)$, it is useful to monitor the entropies of the solid phase (S_S) and the liquid phase (S_L) at the melting point. For the original MEAM potential model, the overestimate of L is largely due to the underestimate of S_S (by 12%), which suggests that the gold crystal model is too 'rigid'. In other words, the anharmonic effect is not large enough to increase the entropy of the solid phase at high temperatures. This is much more improved in the 2nn-MEAM model which uses a smoother many-body screening function. While the melting point of the more recent 2nn-MEAM potential for gold is much closer to the experimental value, the error in the latent heat is still similar to that of the original MEAM potential. We

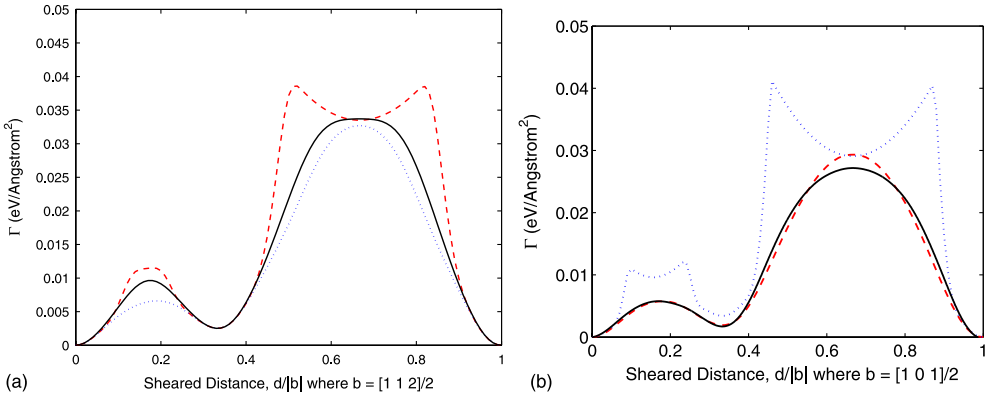

Figure 1. GSF energy of different potential models for gold: (*a*) 2nn-MEAM [26] (dashed line), 2nn-MEAM* (dotted line) and 2nn-MEAM† (solid line); (*b*) EAM [23] (dashed line), MEAM [6] (dotted line) and DFT/LDA (solid line). (Color Online.)

would like to have a better fit to both the melting point and the latent heat by adjusting the 2nn-MEAM gold potential.

Table 1 also lists the predicted values of several other properties that either are important for certain aspects of nanowire growth or are included to illustrate the problem of MEAM potentials. For example, diffusion in the liquid phase may be the rate limiting step in nanowire growth under certain experimental conditions. The mismatch in the thermal expansion coefficient α of gold and silicon can generate internal stress during rapid heating or cooling of the nanowire. The gross underestimate of α in solid gold confirms the above hypothesis that the anharmonic effect is not large enough in the original MEAM potential. The ideal shear strength τ_c can influence the probability of twinning in the gold crystal when the catalyst droplet solidifies during rapid cooling. The volume change on melting $\Delta V_m / V_{solid}$ can generate internal stresses upon melting.

Artifacts of both original and 2nn-MEAM potentials are most clearly shown by the (relaxed) generalized stacking fault (GSF) energy on the (1 1 1) face in the $[1\,1\,\bar{2}]$ shear direction, as shown in figures 1(*a*) and (*b*). We followed the procedures in [20] to compute the GSF curves. The unphysical local minima and cusps on the GSF curve indicate problems for these MEAM potentials, because the GSF curve is expected to be a smooth curve, as predicted by *ab initio* calculations using the density functional theory (DFT) shown in figure 1(*b*). The maximum slope of the GSF curve between zero and the first local minimum is defined as the ideal shear strength τ_c. 2nn-MEAM prediction of τ_c is about a factor of three too high compared with *ab initio* results. The overestimate of L and τ_c suggests a fundamental problem in the 2nn-MEAM potential for gold, which we will address in section 3.

2.2. *Limitations of MEAM silicon potentials*

Table 2 shows that the original MEAM silicon potential [6] underestimates the melting point T_m by ∼270 K (16%) and underestimates the latent heat L by ∼13 kJ mol^{-1} (27%). These are the main problems that we will address in this paper. There is error cancellation in the prediction of latent heat L, because both solid entropy S_S and liquid entropy S_L are underestimated. Contrary to the case of gold, the more recent 2nn-MEAM potential for silicon predicts a much more accurate latent heat but grossly overestimates the melting point (by ∼1000 K). We would like to have a better fit to both the melting point and the latent heat.

Table 2. Model predictions and experimental data [15, 16, 10] of thermal and mechanical properties of silicon. The ideal shear strength [20] obtained from first-principles calculation is also presented for comparison. The computational models include the original MEAM [6] and MEAM 2nn [22]. Superscripts * and † represent modifications to these models introduced in this work. SW [4] and Tersoff [5] models are also included for comparison. The variables and their units are identical to those in table 1.

Si	T_m	L	S_S	S_L	D	α	τ_c	$\Delta V_m/V_{solid}$
MEAM [6]	1411	36.8	48.7	74.8	4.8	13.6	13.8	−5.3
MEAM*	1377	36.7	48.0	74.7	6.3	13.6	13.8	−5.2
MEAM†	1687	43.1	53.7	79.2	7.9	13.2	14.0	−2.7
SW	1695	31.2	58.0	76.5	6.0	3.9	8.9	−6.1
Tersoff	2606	42.3	68.9	85.1	2.5	6.5	18.5	−1.6
2nn-MEAM [22]	2837	49.3	72.9	90.3	6.25	5.2	13.6	−7.5
Exp't	1685	50.2	61.8	91.6	∼10	2.6	—	−5.1
DFT/LDA(GGA)	—	—	—	—	—	—	14.0(13.7)	—

Table 2 also lists the predicted values of several other properties that are included in the benchmark of gold potentials in table 1. Unlike the case of gold, the underestimate of the solid entropy by the MEAM potential [6] is accompanied by a gross overestimate (instead of an underestimate) of the thermal expansion coefficient α. Unfortunately, this is a problem that we are not able to fix in this paper (see section 3). Figure 2(*a*) plots the (relaxed) GSF energy of silicon on the shuffle-set (1 1 1) plane in the [1 $\bar{1}$ 0] shearing direction. While the original MEAM potential predicts some unphysical oscillations, the local minima and cusps in the gold GSF curve are no longer present. The unphysical oscillations become even more severe in the 2nn-MEAM potential [6], indicating an underlying problem. The maximum slope of the GSF curve is the ideal shear strength τ_c, the MEAM prediction of which agrees well with the *ab initio* results. Table 2 also lists the benchmark data for two other commonly used potentials: SW and Tersoff. None of the existing potentials can describe both the melting point and the latent heat accurately. This indicates that it is very difficult to describe both the solid phase and the liquid phase of silicon using an empirical potential, because silicon transforms from a semiconductor to a metal when it melts. In section 3, we describe our approach to improve the MEAM potential for silicon.

3. Methods and results

The main goal of this paper is to improve the melting point and the latent heat predictions of existing MEAM potentials of gold and silicon, by adjusting some of their parameters without changing the overall functional form. The parameters we will adjust should not affect most of the previously fitted properties, such as equilibrium lattice constant, cohesive energy and elastic constants. In this work, we choose to adjust (1) the multi-body screening function and (2) the pair potential function through the EOS. Because the dependence of thermal properties on these parameters is not obvious, the adjustment of the potential proceeds by trial and error, which requires rapid calculation of the melting point and the latent heat for each trial potential. This is done using a newly developed free-energy method [27]. Many physical properties are monitored during the process. Diffusion coefficient D, thermal expansion coefficient α, volume change on melting $\Delta V_m/V_{solid}$ and radial distribution function $g(r)$ are computed by using NPT MD simulations [10]. First, by adjusting the parameter C_{min} in the multi-body screening function, we obtain the potentials for gold and silicon that are marked as MEAM* in tables 1 and 2. Second, by modifying the EOS, we obtain the potentials marked as MEAM†

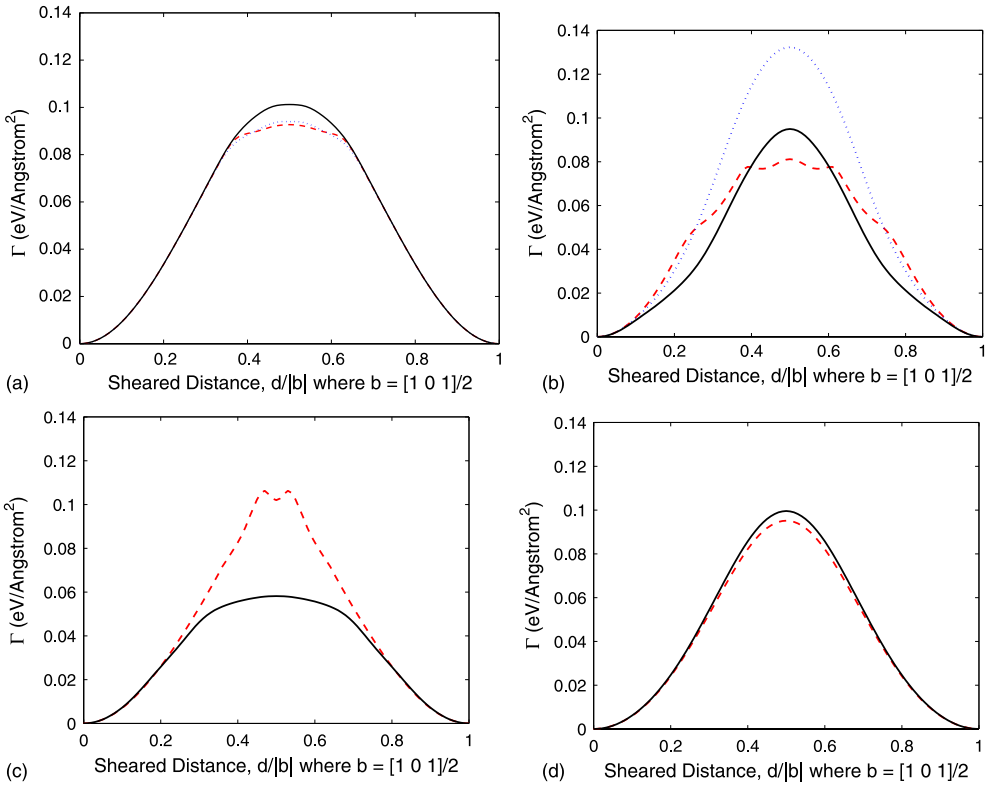

Figure 2. GSF energy of different potential models for silicon. (*a*) MEAM [6] (dashed curve), MEAM* (dotted curve), MEAM† (solid curve); (*b*) 2nn-MEAM [22] (dashed curve); (*c*) Tersoff [5] (solid curve); SW [4] (dashed curve); (*d*) DFT/LDA [20] (solid curve), DFT/GGA [20] (dashed curve). (Color Online.)

that have much better melting point and latent heat predictions. Some other transport and mechanical properties are also improved by the MEAM† models. In a future paper, we will develop gold–silicon cross-potentials based on the MEAM† potentials.

3.1. Multi-body screening function

In this section, we will discuss the physical basis for the need to change the $C_{\min}$ parameter in the multi-body screening function from its original value of 2.0 to a lower value of 0.8 for Au and 1.85 for Si. The multi-body screening function in MEAM allows the interaction between two atoms i and k to be screened by a third atom j. The behavior of the multi-body screening function is controlled by two parameters: $C_{\min}$ and $C_{\max}$ (for more details see appendix A). The default value of $C_{\max}$ is 2.8, which ensures that first nearest-neighbor interactions are completely unscreened even for reasonably large thermal vibrations. In the original MEAM model, $C_{\min}$ is set to 2.0. As a result, in most crystal structures the 2nn interactions are always screened by another atom. Hence the interactions are effectively cut off to within the first nearest-neighbors. In the 2nn-MEAM model, $C_{\min} = 1.53$ for Au and $C_{\min} = 1.41$ for Si are used to improve properties such as the thermal expansion coefficient and vacancy formation energy. However, as shown in the figures 1(*a*) and the 2(*b*), it still has a problem in predicting the GSF energy curve.

Lowering $C_{\min}$ to 0.8 effectively unscreens the 2nn interactions, and has been found to improve several predictions of the MEAM model for FCC Ni, including the thermal expansion coefficient α [19]. The beneficial effects of this adjustment have also been reported for the MEAM models of other FCC metals and BCC metals [27]. For example, the original MEAM model for BCC metals predicts an incorrect ordering of the surface energies of low index surfaces. It also predicts another structure to be more stable than BCC [24], as well as anomalously low melting points [27]. By lowering $C_{\min}$, which effectively extends the interaction to second nearest-neighbors, the predictions of surface energy, thermal expansion coefficient [24, 25] as well as melting points [27] of BCC metals are significantly improved.

Therefore, our first step is to set $C_{\min} = 0.8$ in gold 2nn-MEAM potential and $C_{\min} = 1.85$ in silicon MEAM potential. The resulting potentials are indicated by superscript * in tables 1 and 2 (other parameters are not changed). The latent heat L and the volume change on melting $\Delta V_{\mathrm{m}}/V_{\mathrm{solid}}$ for the 2nn-MEAM* gold potential are significantly improved, indicating that the model now describes the physics of gold more accurately. The artificial metastable states and cusps in the GSF curve are completely removed (dotted line in figure 1(*a*)). The maximum slope of the GSF curve, i.e. the ideal shear strength τ_{c}, becomes very close to the *ab initio* result. We find that these artificial features persist if $C_{\min} > 0.8$, whereas elastic constants and vacancy formation energy will start to change if $C_{\min} < 0.8$. Hence $C_{\min} = 0.8$ seems to be an optimal choice for MEAM gold. However, setting $C_{\min} = 0.8$ significantly decreases the melting point (now about 160 K lower than the experimental value) and increases the thermal expansion coefficient (now about 40% higher than the experimental value). This problem will be addressed in the next section by adjusting the pair potential function.

On the other hand, changing $C_{\min}$ for Si has a negligible effect on the melting point T_{m}, latent heat L, solid entropy S_{S}, liquid entropy S_{L} and thermal expansion coefficient α. This is because the multi-body screening function has a very small effect in the open structure of a diamond-cubic crystal, as explained in appendix A. However, we find that the liquid volume is selectively increased as $C_{\min}$ is lowered, reducing the magnitude of $\Delta V_{\mathrm{m}}/V_{\mathrm{solid}}$. Because $\Delta V_{\mathrm{m}}/V_{\mathrm{solid}}$ is already close to experiment for original MEAM Si, we lower $C_{\min}$ just enough to remove the artificial oscillations in the GSF curve (figure 2(*a*)). The optimal value we converge to is $C_{\min} = 1.85$ for silicon, corresponding to MEAM* in table 2. Hence, we will set $C_{\min} = 0.8$ for gold and $C_{\min} = 1.85$ for silicon in the following discussions.

3.2. Pair potential and EOS

In this section, we adjust the pair potential function of the MEAM potential to fit the melting point and the latent heat of gold and silicon. As mentioned in section 2, the pair potential in the MEAM models is not given explicitly, but is specified in such a way that, when combined with the embedding function, it reproduces the EOS for the reference crystal structure. Hence modifying the pair potential amounts to changing the EOS function, which in the original MEAM potential is expressed as

$$E^{\mathrm{u}}(r) = -E_{\mathrm{c}}\left(1 + a^*\right)\exp(-a^*) \tag{2}$$

with

$$a^* = \left(\frac{9\,\Omega B}{E_{\mathrm{c}}}\right)^{1/2}\left(\frac{r}{r_{\mathrm{e}}} - 1\right), \tag{3}$$

where r is the nearest-neighbor distance of the reference structure [21]. E_{c} is the cohesive energy, r_{e} is the equilibrium nearest-neighbor distance, Ω is the atomic volume and B is the bulk modulus of the reference structure.

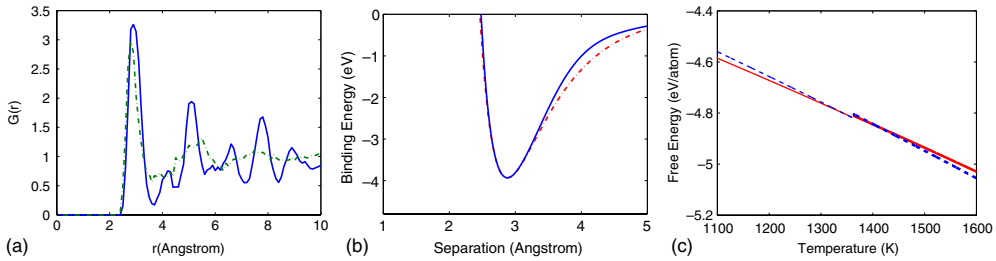

Figure 3. (*a*) Pair-correlation functions of the solid (solid line) and liquid (dotted line) phases of gold described by the 2nn-MEAM [26] potential at its melting point. (*b*) The EOS function in the 2nn-MEAM (dotted line) potential and the new 2nn-MEAM† potential (solid line). (*c*) The Gibbs free energy of the 2nn-MEAM (thick lines) and 2nn-MEAM† (thin lines) potentials for gold; solid lines for the solid phase and dashed lines for the liquid phase. (Color Online.)

Since the MEAM* potentials underestimate the melting points, we need to increase the Gibbs free energy of the liquid phase more than that of the solid phase. An effective way to modify the free-energy difference between the two phases is to change the EOS function at distances r where the radial distribution function $g(r)$ of the two phases differs the most. At the same time, the modified EOS function must not change its value and first and second derivatives at $r = r_e$ because they have been fitted to physical properties. Specifically, $E^u(r_e) = -E_c$, $dE^u/dr|_{r_e} = 0$ and $d^2E^u/dr^2|_{r_e} = 18\,\Omega\,B/r_e^2$. In the following, we will show that the same kind of modifications of the EOS function can be applied to gold and silicon, in order to fit their melting point and latent heat.

3.2.1. 2nn-MEAM† gold potential. Figure 3(*a*) plots the radial distribution function $g(r)$ for the solid and liquid phases of gold using the 2nn-MEAM potential at the melting point. The $g(r)$ for the liquid phase is greater than that in the solid phase at distances between 3.5 and 4.5 Å. Hence the free energy of the liquid phase can be raised more than that of the solid phase by increasing the pair potential energy in this range. A naive approach to modify the EOS function is to add higher order polynomials in the pre-exponential term. Unfortunately, this approach cannot introduce sufficient changes in the melting point without creating unphysical oscillations in the EOS function. By trial and error, we find that the form of the EOS function leads to the desired changes in the melting point.

$$E^u(r) = -E_c\left(1 + a^* + da^{*3} + \gamma\, a^{*4} e^{-\lambda a^{*2}}/r\right) \exp(-a^*) \tag{4}$$

da^{*3} is a small correction term added in 2nn-MEAM Au potential [26] with $d = 0.05\,\text{Å}^{-3}$. The higher order term a^{*4} is multiplied by an exponential $e^{-\lambda a^{*2}}/r$ to remove unphysical oscillations in the range of $r > r_e$. For each pair of trial values (γ, λ), we re-compute the free energies of the liquid and solid phases using the method described in [27]. It turns out to be very difficult to find a parameter set that simultaneously fits the experimental melting point and latent heat. Hence a compromise must be reached. The 'optimal' values we converge to are $\gamma = -0.182\,\text{Å}$ and $\lambda = 4.0$. The resulting EOS and free energies are plotted in figures 3(*b*) and (*c*), respectively. The thermal and mechanical properties of the resulting potential, 2nn-MEAM†, are listed in table 1. The melting point is very close to experimental value, and the latent heat is significantly improved over the original 2nn-MEAM. Unfortunately, the maximum slope of the GSF curve, i.e. the ideal shear strength τ_c, is now about 60% bigger than the *ab initio* results. The GSF energy for the 2nn-MEAM† model is plotted in figure 1(*a*).

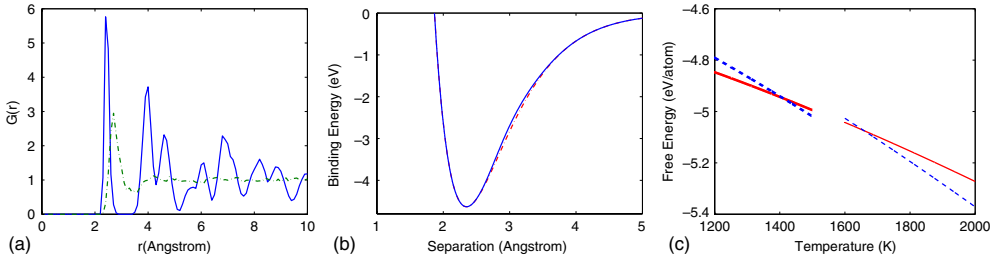

Figure 4. (*a*) Pair-correlation functions of the solid (solid line) and liquid (dotted line) phases of silicon described by the MEAM [6] potential at its melting point. (*b*) The EOS function in the original MEAM (dotted line) potential and the new MEAM† potential (solid line). (*c*) The Gibbs free energy of the MEAM (thick lines) and MEAM† (thin lines) potentials for silicon; solid lines for the solid phase and dashed lines for the liquid phase. (Color Online).

The 2nn-MEAM* model has better GSF curves and volume change on melting than the 2nn-MEAM† model. But the 2nn-MEAM† model has more accurate melting point and latent heat. We believe the latter is a better candidate on top of which we can construct a gold–silicon cross-potential for the purpose of VLS nanowire growth modeling.

3.2.2. MEAM† silicon potential. Figure 4(*a*) plots the radial distribution function $g(r)$ for the solid and liquid phases of silicon using the original MEAM potential at the melting point. The $g(r)$ of liquid is higher than that of solid at distances between 3 Å and 3.5 AA. We found that the following form of the EOS function leads to desirable changes of the melting point:

$$E^{\mathrm{u}}(r) = -E_{\mathrm{c}}\left(1 + a^* + \gamma\, a^{*4}\mathrm{e}^{-\lambda a^{*2}}/r\right)\exp(-a^*) \tag{5}$$

where the 'optimal' values we found are $\gamma = -0.36$ Å and $\lambda = 16.0$. The resulting EOS and free energies are plotted in figures 4(*b*) and (*c*), respectively. The thermal and mechanical properties of the resulting potential, MEAM†, are listed in table 2. The melting point and the latent heat of the MEAM† Si potential are now both close to the experimental values. The GSF curve for the MEAM† model, as shown in figure 2(*c*), becomes closer to the *ab initio* results with negligible change in ideal strength τ_{c}. The diffusion coefficient of liquid is also improved.

However, the MEAM† silicon potential still has problems on properties other than the melting point and the latent heat. Both solid and liquid entropies are underestimated; their cancellation of error leads to a better agreement of the latent heat with experiments. The thermal expansion coefficient of solid remains too high, similar to the original MEAM potential. The volume change on melting becomes a factor of two smaller than experiments. In addition, the first and second highest peaks of the liquid $g(r)$ occurs at 2.7 Å and 4.2 Å, respectively, deviating from the experimental values of 2.50 Å and 3.78 Å [28]. This problem existed in the original MEAM model and our modifications do not change the location of these peaks significantly. Nonetheless, most of the problems listed above (except the entropies) do not affect the thermodynamic behavior of the potential model. With a more accurate fit to the melting point and the latent heat, the MEAM† silicon potential is a better candidate than the original MEAM silicon potential, on top of which we can construct a gold–silicon cross-potential that can be fitted to the binary phase diagram. We have also applied the same approach to adjust the 2nn-MEAM potential for silicon. Unfortunately, we have not succeeded in reproducing both the melting point and the latent heat to the same level of agreement with experiments as in the MEAM† potential.

4. Summary

We have adjusted the MEAM potentials for gold and silicon, two elements with fundamentally different bonding mechanisms, to fit the melting point and the latent heat more accurately, by changing the multi-body screening function and the EOS function. For both gold and silicon, the melting point and the latent heat values are now close to the experimental values. The thermal expansion coefficient and GSF curve for gold are significantly improved, mostly by changing $C_{\min}$ to 0.8 in the multi-body screening function. The thermal expansion coefficient for silicon is insensitive to the adjustments considered in this paper and remains too high compared with experiments. In appendix B we provide more benchmark data of the modified potentials. Table B1 lists the elastic constants, defect energy and surface energies, which are not very different from the original MEAM potentials. The bond angle distribution in liquid silicon also agrees well with the *ab initio* results. The resulting MEAM† models for gold and silicon provide a good basis for constructing a cross-potential model which can be fitted to the binary gold–silicon phase diagram. Since we have not changed most of the MEAM parameters, it is possible that by fitting these parameters again one may obtain a better agreement with experimental values.

Acknowledgments

This work is partly supported by the DOE/SciDAC project on Quantum Simulation of Materials and Nanostructures and NSF/CMMI Nano Bio Materials Program CMS-0556032. SR and CRW acknowledges support from the Stanford Graduate Fellowship Program.

Appendix A. Multi-body screening function

In this appendix, we give a brief summary of the multi-body screening function in the MEAM potential and describe why lowering $C_{\min}$ has a beneficial effect on many structural properties for Au. Consider a pair of atoms i and k. The interaction between the two is screened by a factor S_{ik}. If $S_{ik} = 1$ then the interaction is not screened; if $S_{ik} = 0$ then the interaction is completely screened. S_{ik} depends on the distribution of atoms j that are common neighbors of i and k;

$$S_{ik} = \prod_{j \neq i,k} S_{ijk}. \tag{A.1}$$

The functional form of S_{ijk} is constructed based on the idea that the closer atom j is to the segment (i.e. bond) connecting atoms i and k, the more effectively it screens their interaction. On the plane that simultaneously contains atoms i, j and k, define a local coordinate system x–y such that the origin lies at the mid-point between i and k, and the x-axis points from i to k. Let r_{ik} be the distance between atoms i and k and introduce scaled coordinates $X = x/r_{ik}$ and $Y = y/r_{ik}$. Now imagine a series of ellipses that pass through atoms i and k, as shown in figure A1, and parametrized by the following equation:

$$X^2 + \frac{Y^2}{C} = \frac{1}{4}. \tag{A.2}$$

The parameter C controls the extension of the ellipse along the y-axis. If the ellipse passes through atom j, then

$$C = \frac{2(X_{ij} + X_{jk}) - (X_{ij} - X_{jk})^2 - 1}{1 - (X_{ij} - X_{jk})^2}, \tag{A.3}$$

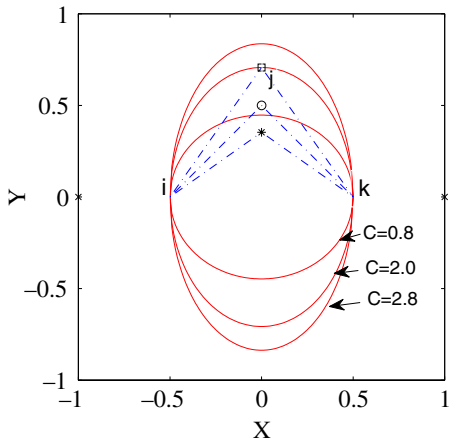

Figure A1. Ellipses defined in equation (A.2) for different values of C (0.8,2.0,2.8). The line segments represent nearest-neighbor bonds i–j and j–k in BCC (square), FCC (circle) and diamond-cubic (asterisk) crystal structures, scaled by the 2nn distance r_{ik}. In these three crystal structures, the atom j lies on the ellipses (not shown) corresponding to $C = 0.5$, 1.0 and 2.0, respectively. (Color Online.)

where $X_{ij} \equiv (r_{ij}/r_{ik})^2$ and $X_{jk} \equiv (r_{jk}/r_{ik})^2$. Figure A1 plots the ellipses when $C = 0.5$, $C = 2.0$ and $C = 2.8$. In MEAM, one specifies the screening factor in terms of two parameters, $C_{\max}$ and $C_{\min}$. When atom j lies outside the ellipse defined by $C = C_{\max}$, $S_{ijk} = 1$; when atom j lies inside the ellipse defined by $C = C_{\min}$, $S_{ijk} = 0$. When atom j lies in between these two ellipses, S_{ijk} is between 0 and 1 and is a smooth function of the coordinates of atom j. This can be achieved by introducing a cut-off function:

$$f_c(x) = \begin{cases} 1 & x \geqslant 1, \\ (1-(1-x)^4)^2 & 0 < x < 1, \\ 0 & x \leqslant 0, \end{cases} \tag{A.4}$$

and let

$$S_{ijk} = f_c\left(\frac{C - C_{\min}}{C_{\max} - C_{\min}}\right). \tag{A.5}$$

The consequences of the choices of $C_{\max}$ and $C_{\min}$ can be seen by analyzing the geometry of perfect crystals. For example, consider an FCC lattice. If atoms i and k are second nearest-neighbors, and atom j is their common first nearest-neighbor, then $C = 1.0$. Hence the choice of $C_{\min} = 2.0$ in the original MEAM model means that the interaction between second nearest-neighbors in FCC crystals is completely screened. Unfortunately, cutting off the interaction between second nearest-neighbors leads to cusps in the GSF energy as well as a very small thermal expansion coefficient. Reducing $C_{\min}$ to 0.8 extends the interaction range beyond second nearest-neighbors and removes these artifacts for FCC gold.

Now consider the diamond-cubic structure. If atoms i and k are second nearest-neighbors, and atom j is their common first nearest-neighbor, then $C = 0.5$. Hence 2nn interactions in crystalline silicon is cut off even for very large thermal vibration at high temperatures. This is why lowering $C_{\min}$ from 2.0 to 0.8 has hardly any effect for the solid phase of silicon. However, the properties of the liquid phase is affected by this change because the interaction range between atoms is effectively enlarged. In this paper, we change $C_{\min}$ of Si to 1.85.

Table B1. The elastic constants, C_{11}, C_{12} and C_{44} (in GPa), vacancy formation energy E_v (in eV) and surface energies E_{100}, E_{110} and E_{111} (in erg cm^{-2}) from experimental measurements [6, 29, 31, 32], first-principles calculations [30, 31, 34, 35] (except silicon elastic constants computed here using DFT/LDA) and various MEAM models considered in this paper. The unrelaxed energies are given in parentheses. The DFT results are from several different pseudopotentials. Surface reconstruction such as dimer structure is not considered in the calculation of relaxed surface energy of silicon.

	C_{11}	C_{12}	C_{44}	E_v	E_{100}	E_{110}	E_{111}
Au							
2nn-MEAM	201.5	169.7	45.4	0.91(0.96)	1083(1138)	1045(1179)	903(928)
2nn-MEAM*	201.5	169.7	45.4	0.91(0.96)	1083(1138)	1045(1178)	903(928)
2nn-MEAM†	202.1	169.5	45.4	0.91(0.96)	1084(1138)	1048(1179)	903(928)
Exp't	201.6	169.7	45.4	0.94	1540(poly)	—	—
DFT	217	171	47	0.55	1968	1098	917
Si							
MEAM	164	65	76	3.28(4.04)	1742(1850)	1413(1536)	1195(1254)
MEAM*	164	65	76	3.28(4.04)	1742(1850)	1413(1536)	1195(1254)
MEAM†	164	65	76	3.56(4.06)	1744(1851)	1414(1536)	1196(1254)
Exp't	165.8	63.5	79.6	—	1135(poly)	—	—
DFT	158	65	77	2.7–3.9	2683(2716)	—	1741(1954)

Appendix B. Further benchmarks of the MEAM† potentials

Even though we have modified the multi-body screening function and the EOS, the elastic moduli, vacancy formation energy and surface energies are not changed significantly from the original MEAM potentials, as shown in table B1. The changes of elastic and defect properties are very small for the following reasons. First, while lowering $C_{\min}$ extends the interaction to second nearest-neighbors, these interactions are much weaker than the first nearest-neighbor interactions. Second, the modification of the EOS is appreciable only at distances well beyond the equilibrium nearest-neighbor distance. The effects on the elastic moduli, vacancy formation energy and surface energies are negligible because they are dominated by nearest-neighbor interactions.

Because we choose to change only a few parameters in the existing MEAM models, our models share some of the same limitations of the existing models. One limitation is the prediction of Si surface structure. First, the unrelaxed surface energy is about 30% lower than the *ab initio* results. While the MEAM potential correctly predicts the 2×1 reconstruction of the {1 0 0} surface [22], it does not predict the (7×7) reconstruction of the {1 1 1} surface as observed in experiments [36] and *ab initio* simulations [37]. The MEAM† potential predicts similar energies for the 3×3, 5×5, 7×7, 9×9 reconstructed {1 1 1} surface as the original MEAM potential. A previous report [38] claimed that the original MEAM silicon potential predicts the (7×7) reconstruction as the ground state of the {1 1 1} surface. This is incorrect because the reconstructed surface energy (1524 erg cm^{-2}) is much higher than the unreconstructed surface energy (1254 erg cm^{-2}) [6].

Contrary to the case of Si, the MEAM Au potentials reproduce very well the energies predicted by DFT for the {1 1 0} and {1 1 1} surfaces. A large gap is still observed for the {1 0 0} surface.

We also compared the bond angle distribution $g_3(\theta, r_m)$ of the silicon liquid described by MEAM†, *ab initio* [33] and SW models [33] in figure B1. The average coordination numbers from the *ab initio* and SW model are 6.5 and 4.9 at 1800 K, respectively [33].

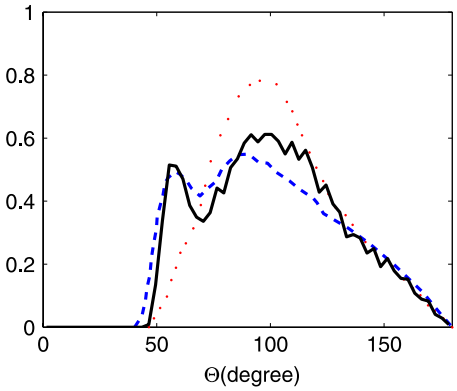

Figure B1. Bond angle distribution functions of liquid phase of silicon described by the MEAM† (solid line), DFT/LDA (dashed line) [33] and SW (dotted line) [33]. (Color Online.)

$r_{\mathrm{m}} = 3.15\,\text{Å}$ is taken to be the first local minima of the radial distribution $g(r)$ in our calculation. The simulation is performed at the melting point of the MEAM† model, which is 1687 K. The MEAM† model predicts two peaks in the $g3(\theta, r_m)$ plot, consistent with the *ab initio* simulations. In comparison, this feature is absent in the SW model of Si, as shown in figure B1. The average number of neighbor atoms within a cut-off radius of r_{m} (i.e. the coordination number) is 5.7 for the MEAM† model. In comparison, the coordination number for the original MEAM potential is 6.6 at its melting temperature of 1411 K. Hence the MEAM† model provides a reasonable description of the solid and liquid properties of silicon.

References

[1] Lieber C M and Wang Z L 2007 *MRS Bull.* **32** 99
[2] Wong H-S P 2002 *IBM J. Res. Dev.* **46** 133
[3] Daw M S and Baskes M I 1983 *Phys. Rev. Lett.* **50** 1285
[4] Stillinger F H and Weber T A 1985 *Phys. Rev.* B **31** 5262
[5] Tersoff J 1986 *Phys. Rev. Lett.* **56** 632
[6] Baskes M I 1992 *Phys. Rev.* B **46** 2727
[7] Lee B 2006 *Acta Mater.* **54** 701
[8] Lee B, Wirth B D, Shim J, Kwon J, Kwon S and Hong J 2005 *Phys. Rev.* B **71** 184205
[9] Kim Y and Lee B 2007 *Mater. Sci. Eng.* A **449** 733
[10] Cook S J and Clancy P 1993 *Phys. Rev.* B **47** 7686
[11] Zhang J M, Ma F and Xu K W 2004 *Appl. Surf. Sci.* **229** 34
[12] Grochola G, Russo S P, Yarovsky I and Snook I K 2004 *J. Chem. Phys.* **120** 3425
[13] Creemers C, Deurinck P, Helfensteyn S and Luyten J 2003 *Appl. Surf. Sci.* **219** 11
[14] Wang G F, Van Hove M A, Ross P N and Baskes M I 2005 *Prog. Surf. Sci.* **79** 28
[15] Lide D R 2007–2008 *CRC Handbook of Chemistry and Physics* 88th edn (New York: CRC Press)
[16] Barin I 1989 *Thermochemical Data of Pure Substances* (Weinheim: VCH)
[17] Brandes E A and Brook G B 1992 *Smithells Metals Reference Book* 7th edn (Oxford: Butterworth-Heinemann)
[18] The Vienna Ab initio Simulation Package (VASP) http://cms.mpi/univie.ac.at/vasp/
[19] Baskes M I 1997 *Mater. Chem. Phys.* **50** 152
[20] Kang K and Cai W 2007 *Phil. Mag.* **87** 2169
[21] Rose J H, Smith J R, Guinea F and Ferrante J 1984 *Phys. Rev.* B **29** 2963–9
[22] Lee B-J 2007 *Computer Coupling of Phase Diagrams and Thermochemistry* **31** 95–104
[23] Park H S and Zimmerman J A 2005 *Phys. Rev.* B **72** 054106
[24] Lee B and Baskes M I 2000 *Phys. Rev.* B **62** 8564
[25] Lee B, Baskes M I, Kim H and Cho Y K 2001 *Phys. Rev.* B **64** 184202
[26] Lee B, Shim J-H and Baskes M I 2003 *Phys. Rev.* B **68** 144112

[27] Ryu S and Cai W 2008 *Modelling Simul. Mater. Sci. Eng.* **16** 085005
[28] Waseda Y and Suzuki K 1975 *Z. Phys.* B **20** 339
[29] Hirth J P and Lothe J 1992 *Theory of Dislocations* 2nd edn (Malabar, FL: Krieger Publishing)
[30] Justo J F, Bazant M Z, Kaxiras E, Bulatov V V and Yip S 1993 *Phys. Rev.* B **58** 2539
[31] Oliver S, Conte R and Fortunelli A 1994 *Phys. Rev.* B **77** 054104
[32] Tyson W R and Miller W A 1977 *Surf. Sci.* **62** 267
[33] Stich I, Car R and Parrinello M 1991 *Phys. Rev.* B **44** 4262
[34] Yin M T and Cohen M L 1981 *Phys. Rev. Lett.* **24** 2303
[35] Balamane H, Halicioglu T and Tiller W A 1992 *Phys. Rev.* **46** 2250
[36] Takayanagi K, Tanishiro Y, Takahashi M and Takahashi S 1985 *J. Vac. Sci. Technol.* A **3** 1502
Takayanagi K, Tanishiro Y, Takahashi M and Takahashi S 1985 *Surf. Sci.* **164** 367
[37] Brommer K D, Needels M, Larson B E and Joannopoulos J D 1992 *Phys. Rev. Lett.* **68** 1355
[38] Takahashi K, Nara C, Yamagishi T and Onzawa T 1999 *Appl. Surf. Sci.* **151** 299